

Detailed near-infrared study of the ‘water’-related transformations in silcrete upon heat treatment

Patrick Schmidt^{1,2}  · Christoph Lauer² · Gerald Buck² · Christopher E. Miller³ · Klaus G. Nickel²

Received: 21 March 2016 / Accepted: 28 July 2016
© Springer-Verlag Berlin Heidelberg 2016

Abstract In archaeology, lithic heat treatment is the process of modifying a rock for stone tool production using fire. Although the earliest known cases of heat treatment come from South Africa and involved silcrete, a microcrystalline pedogenic silica rock, its thermal transformations remain poorly understood. We investigate the ‘water’-related transformations in silcrete using direct transmission near-infrared spectroscopy. We found that SiOH is noticeably lost between 250 and 450 °C and hydroxyl reacts with H₂O, part of which is trapped in the structure of the rocks. This water can only be evaporated through heat-induced fracturing at high temperatures, imposing maximum temperatures for silcrete heat treatment of approximately 500 °C. Between 250 and 450 °C new siloxane bonds are formed according to the reaction $2\text{SiOH} \rightarrow \text{Si-O-Si} + \text{H}_2\text{O}$, which can be expected to transform the rock’s mechanical properties. The tolerance of silcrete for relatively fast ramp rates can be explained by its pore volume and low SiOH content, ensuring good water evaporation.

These results shed light on the processes taking place in silcrete during heat treatment and allow for a better understanding of the parameters needed for it.

Keywords Lithic heat treatment · Thermal transformations · Silica rocks · Near FTIR · South African silcrete MSA heat treatment

Introduction

In archaeology, lithic heat treatment is the process of intentionally altering a rock to improve its knapping quality for stone tool production. The technique was first applied in southern Africa during the Middle Stone Age (Brown et al. 2009; Mourre et al. 2010; Porraz et al. 2013; Schmidt and Mackay 2016; Schmidt et al. 2015), and it is known from the European Upper Palaeolithic and Mesolithic (Bordes 1969; Eriksen 2006; Tiffagom 1998), the American Paleo-Indian period (Crabtree and Butler 1964; Wilke et al. 1991) and the European Neolithic (Binder 1984; Léa 2005). Understanding the processes involved in heat treatment of stone, such as the nature and parameters of the thermal transformation, is therefore of great importance to the study of stone tool production during these periods. The more recent examples of heat treatment, from Europe or North America, all concern chalcedony-rich rocks such as flint and chert (henceforth only referred to as chert), the thermal transformations of which have been investigated in detail over the past years. These transformations involve the rocks’ silanol (SiOH) content of up to 1 wt% (Flörke et al. 1982; Graetsch et al. 1985; Schmidt et al. 2011), their 0.2–0.5 wt% structural H₂O and their network of intergranular water-adsorbing pores accounting for 0.5–1.5 vol% of the total rock (Fukuda et al. 2009; Micheelsen 1966;

Electronic supplementary material The online version of this article (doi:10.1007/s00269-016-0833-6) contains supplementary material, which is available to authorized users.

✉ Patrick Schmidt
patrick.schmidt@uni-tuebingen.de

¹ Department of Prehistory and Quaternary Ecology, Eberhard Karls University of Tübingen, Schloss Hohentübingen, 72070 Tübingen, Germany

² Department of Geosciences, Applied Mineralogy, Eberhard Karls University of Tübingen, Wilhelmstraße 56, 72074 Tübingen, Germany

³ Institute for Archaeological Sciences, Eberhard Karls University of Tübingen, Rümelinstrasse 23, 72070 Tübingen, Germany

Roqué-Rosell et al. 2010; Schmidt et al. 2011). When heated, the first reaction that begins at 200 °C is the loss of SiOH located on pore walls, followed by the gradual loss of silanol located at defect sites within the rocks (Schmidt et al. 2011, 2012, 2013b). Surface silanol is ‘converted’ to molecular water by the reaction $\text{Si-OH}\cdots\text{OH-Si} \rightarrow \text{Si-O-Si} + \text{H}_2\text{O}$ (Schmidt et al. 2011, 2012), resulting in newly formed Si–O–Si bonds that account for the improved mechanical properties. The ‘water’ content, the amount of pore space and the total volume of the rocks subjected to heat treatment dictate the different parameters of heat treatment such as maximum temperatures or heating rate (Mercieca and Hiscock 2008; Schmidt 2011, 2014; Schmidt et al. 2012). Although we have a relatively good understanding of the thermal transformations of chert, the earliest known examples of lithic heat treatment, dating from the Middle Stone Age of southern Africa, do not involve these types of rocks. Similar to the Australian archaeological record (Cochrane et al. 2012; Corkill 1997; Hanckel 1985; Hiscock 1993; Rowney 1994), the South African record documents heat treatment of silcrete (Brown et al. 2009; Schmidt et al. 2013a). Unlike chert, which is composed of chalcedony (a nano-crystalline fibrous quartz tissue containing silanol at large external and internal surfaces due to intense crystal twinning) (Flörke et al. 1991), most South African silcrete is composed of microquartz, an agglomerate of randomly oriented quartz crystals ranging from a few micrometres to more than a millimetre in size. Such pedogenic silica rocks normally contain two generations of quartz crystals, larger clasts of quartz inherited from the rock that originally formed the regolith and a finer microquartz matrix cementing the clasts together (Summerfield 1983). The most common mineral other than quartz is anatase (TiO_2) with up to 3 wt%; clay may account for 0.5 wt% (Roberts 2003; Summerfield 1983). The nature and structural sites of different ‘water’ species in the microquartz of silcrete remain poorly understood. The available data (Schmidt et al. 2013a) suggest that, like in chalcedony, water is present as H_2O and SiOH, but concentrations are significantly lower in silcrete. The thermal behaviour of SiOH appears to be similar as in chalcedony, even though temperature ranges are different. However, the role of structural H_2O , the evolution of the pore space and the H-bonding behaviour of SiOH and H_2O remain unknown.

In this work, we investigate the role of ‘water’ in silcrete using near-infrared (NIR) spectroscopy (NIR is here defined as the wavenumber range of 7000–4000 cm^{-1} or the wavelength range of 1428–2500 nm. The lower end is imposed by the onset of the black body spectrum in most commercial mid-infrared spectrometers and the upper end is defined as the conventional cut-off wavenumber that marks the beginning of the mid-infrared range). The infrared spectra of quartz show several bands assigned

to H_2O and SiOH: the fundamental vibrations of H_2O cause a broad absorption band in the mid-infrared near 3400 cm^{-1} that interferes with the sharp fundamental O–H stretching vibration of silanol (Aines and Rossman 1984; Frondel 1982). In the NIR region, a SiOH combination mode involving O–H stretching and Si–O–H bending causes a band near 4600 cm^{-1} (Scholze 1960). H_2O causes a ($\nu_2 + \nu_3$) combination band near 5200 cm^{-1} and the first overtone of the H_2O stretching vibration lies near 7000 cm^{-1} (Langer and Flörke 1974). A comprehensive and synthetic overview of all ‘water’ species in quartz is given in Kronenberg (1994). In this study, we use the two NIR combination bands described above but not the H_2O overtone. The frequencies and shapes of these combination bands are sensitive to hydrogen bonding, shifting to lower wavenumbers when these species are involved in H-bonding with neighbouring SiOH or H_2O (Flörke et al. 1982; Graetsch et al. 1985; Langer and Flörke 1974). Langer and Flörke (1974), for example, identified two types of SiOH in opals and showed the NIR combination band to be a convolution of a high-energy component, free from H-bonding and a low-energy component, representing hydrogen-bonded silanol. The frequency of the fundamental OH stretching vibration is also sensitive to hydrogen bonding: the band shifts between 3750 cm^{-1} for isolated and 3500 cm^{-1} for strongly H-bonded groups (Anderson jr 1965; Anderson jr and Wickersheim 1964; Benesi and Jones 1959). Isolated SiOH, not or almost not involved in hydrogen bonding, can be measured through a fundamental OH stretching band at 3740 cm^{-1} (Anderson jr and Wickersheim 1964; Frondel 1982; McDonald 1958).

Based on this infrared signature of water in quartz, we present new data on the process of ‘dehydration’ of microquartz in silcrete upon heat treatment. Our study gives new insight into the thermal response, the loss of silanol, the role of structural water during heat treatment and the evolution of porosity in silcrete.

Samples and experimental protocol

We analysed three samples of silcrete from the West Coast region of South Africa. We chose the samples for our analyses because silcrete from these three outcrops was used in the nearby Middle Stone Age site of Diepkloof Rock Shelter for heat treatment and subsequent stone tool knapping (Porraz et al. 2013; Schmidt et al. 2015). Sample numbers and descriptions as determined by infrared spectroscopy and thin section microscopy are summarised in Table 1.

All samples were cut into sections of approximately 520 μm thickness and diamond polished on both sides. The infrared transmission of these slabs was measured at normal incidence between 5600 and 2600 cm^{-1} with a resolution

Table 1 Sample numbers, descriptions, sample thicknesses, ‘water’ content and pore space (m = mass as determined by the NIR absorption in the dehydrated state)

Sample	Description	Thickness (μm)	m SiOH (wt%)	m H ₂ O (wt%)	Pores (vol%)
WK-13-08	Silcrete with a floating texture. Clasts: 32 vol% with average size 0.2 mm. Crystal size cement >5 μm	520 ± 5	0.43 ± 0.01	0.36 ± 0.01	3.39 ± 0.1
WK-13-11	Silcrete with a floating to grain supported structure. Clasts: 58 vol% with average size 0.19 mm. Crystal size cement $\approx 7 \mu\text{m}$	522 ± 5	0.1 ± 0.01	0.13 ± 0.01	0.69 ± 0.1
WK-13-13	Silcrete with Grain supported structure. Clasts: 66 vol% with average size 0.92 mm. Crystal size cement $\approx 12 \mu\text{m}$	509 ± 5	0.05 ± 0.01	0.09 ± 0.01	0.26 ± 0.1

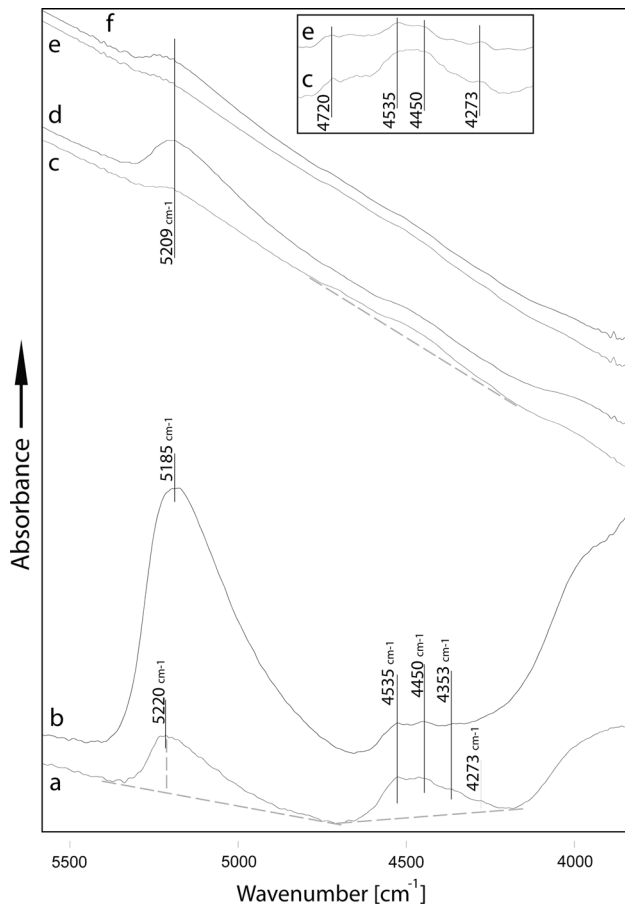


Fig. 1 Room-temperature NIR spectra of the OH region of silcrete samples WK-13-08 (bottom), WK-13-11 (middle) and WK-13-13 (top). *a* WK-13-08 dehydrated spectrum; *b* hydrated; *c* WK-13-11 dehydrated; *d* hydrated; *e* WK-13-13 dehydrated; *f* hydrated. Spectra displaced vertically and acquired at room temperature before heat treatment. The inset shows details of spectra (*c*) and (*e*) after baseline correction for better readability. Note that all absorbances were measured on untreated spectra, i.e. without such baseline subtraction. Baselines used for the absorbance measurements are shown as grey broken lines for spectra (*a*) and (*c*)

of 4 cm^{-1} , using an Agilent Cary 660-IR FTIR spectrometer and unpolarised radiation. The baselines for absorbance measurements of the two combination bands were straight lines between the two lowest points on either side of the

absorption bands (Fig. 1). The baseline for the absorbance measurements of isolated SiOH at 3740 cm^{-1} is shown in Fig. 2e. Error bars for the measured ‘water’ contents were calculated by repeating spectral acquisition and data treatment on each sample for 10 times. For this, each sample was mounted in the spectrometer, a spectrum was acquired, the sample was un-mounted and the procedure was repeated. The so-calculated error bars reflect silcrete’s heterogeneity in terms of OH, i.e. the inner sample variation of the concentration of different ‘water’ species. We calculated the mass (m) of silanol and molecular water in the samples using the molar absorption coefficients given by Scholze (1960) and the formula:

$$m = \frac{MA}{10\rho_{\text{SiO}_2}\alpha d}$$

with M = the molar mass of the water species: 18 g/mol for H₂O and 17 g/mol for OH in silanol; A = absorbance; ρ_{SiO_2} = density of quartz: 2.65 g/cm^3 ; α = Scholze’s absorption coefficient: 1.14 L/mol cm for H₂O and 160 L/mol cm^2 for silanol; d = thickness of the samples in cm. All absorbances were measured directly on the IR spectra without smoothing or baseline subtraction. The H₂O concentration was determined using the linear absorbance measured at 5209 cm^{-1} (WK-13-11 and WK-13-13), 5220 cm^{-1} (WK-13-08 dehydrated) or 5185 cm^{-1} (WK-13-08 hydrated), and the silanol concentration was determined using the integral absorbance of the combination band near 4400 cm^{-1} . However, the so-calculated SiOH contents must be considered as indications only because Scholze specified α for silanol in glass and not for microcrystalline quartz as in silcrete. Refinement of the absorption coefficient of the NIR silanol band in silcrete must await further studies. The comparison of the silanol contents in the three samples and between different temperature steps is nonetheless significant because the same (imprecise) absorption coefficient was used for all of them. The volume of intergranular porosity was calculated as follows: first, pore water at maximum saturation of the samples’ pore space was calculated according to the method described in Schmidt et al. (2011): the quantity of H₂O in the dehydrated state was subtracted from the H₂O content in the hydrated state to obtain H₂O loosely held in

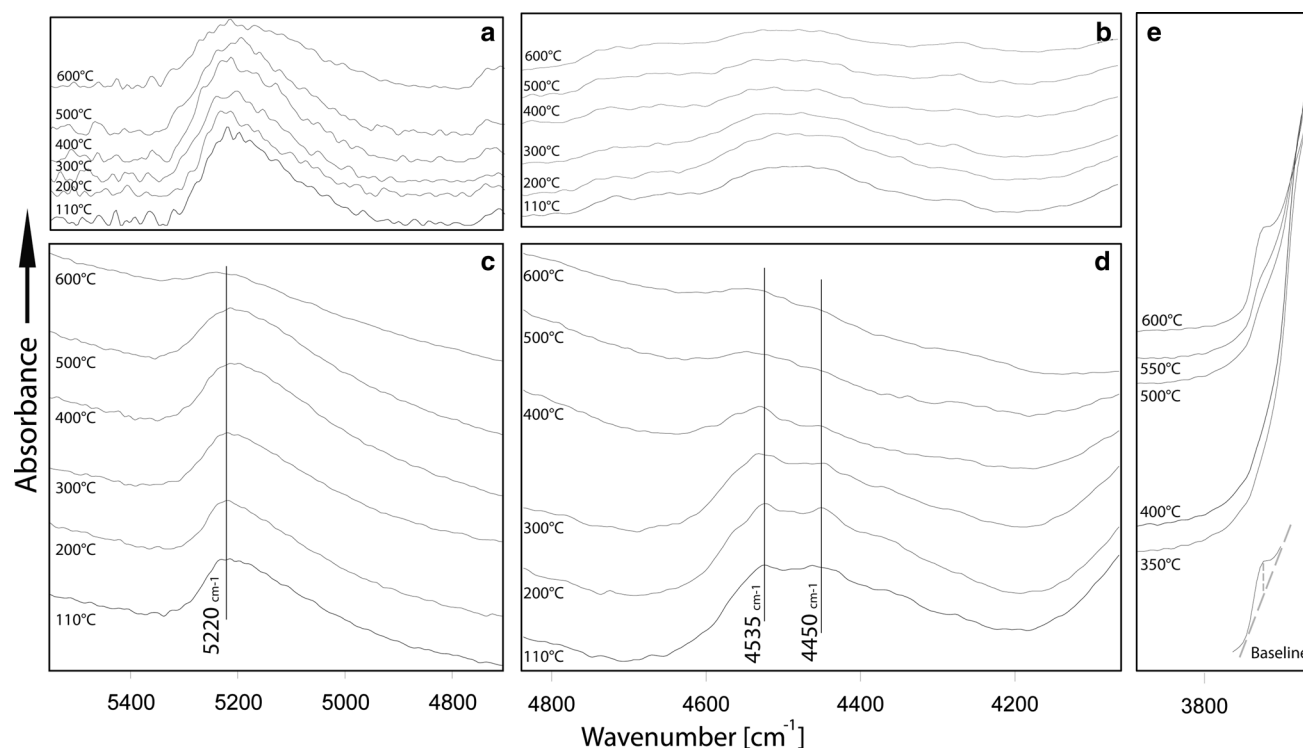


Fig. 2 Spectra recorded at room temperature after heating to different temperatures. **a, b** Evolution of the H₂O (**a**) and the SiOH (**b**) combination bands of WK-13-11 after baseline correction for better readability. Note that all absorbances were measured on untreated spectra, i.e. without such baseline subtraction. **c, d** Evolution of the H₂O (**c**) and the SiOH (**d**) combination bands of WK-13-08. Note the gradual intensity loss of the bands in WK-13-08 and WK-13-11

and the relative change in the intensities of the SiOH bands' different components. The components themselves do not shift in frequency. **e** Spectra of WK-13-08 showing the appearance of the fundamental OH stretching vibration at 3740 cm⁻¹ due to isolated SiOH. The baseline for absorbance measurements at 3740 cm⁻¹ is shown in the lower part of (**e**). All spectra vertically offset for better readability

open pores. The pore space $V_{(\text{pores})}$ in vol% of the rocks was calculated as:

$$V_{\text{pores}} = m_{\text{pH}_2\text{O}} / \left(\frac{100 - m_{\text{TiO}_2} - m_{\text{H}_2\text{O}}}{\rho_{\text{SiO}_2}} + \frac{m_{\text{TiO}_2}}{\rho_{\text{TiO}_2}} + m_{\text{H}_2\text{O}} \right) \times 100$$

with $m_{\text{pH}_2\text{O}}$ = mass of H₂O held in open pores in wt%; m_{TiO_2} = mass of anatase in wt% as determined by semi-quantitative analysis of XRD data; $m_{\text{H}_2\text{O}}$ = mass of H₂O in the hydrated state in wt%; ρ_{SiO_2} = density of quartz; ρ_{TiO_2} = density of anatase. We used an anatase content of 0.5 wt% for all samples [this value was determined for the three samples during our analyses for preparing this study (Lauer 2014)], a density of quartz = 2.62 g/cm³ and a density of anatase = 3.85 g/cm³ for the calculation. Additionally, we calculated the ratio between the intensities of two components of the SiOH combination band (4450 and 4535 cm⁻¹) as a measure of the implication of silanol in H-bonding. Intensity measurements for the ratio calculation were obtained through spectral decomposition of the SiOH band using Lorentzian functions. In order to obtain the two components, the baseline was subtracted and the whole SiOH absorption envelope was fitted with four bands at

4273, 4353, 4450 and 4535 cm⁻¹ for WK-13-08 and at 4273, 4450, 4535 and 4720 cm⁻¹ for WK-13-11 and WK-13-13.

The heating experimental for assessing the thermal evolution of the different OH species was as described in Schmidt et al. (2011): the samples were dehydrated at 110 °C for 48 h in an electrical furnace. Spectra were recorded in the dehydrated state immediately after the samples had cooled to room temperature and before the pore space could reabsorb atmospheric H₂O. The samples were then rehydrated in deionised H₂O for 48 h at room temperature and a second spectrum was acquired in the hydrated state. After this, the samples were heated to 150 °C during 4 h and held at this temperature for another 4 h before the oven was set to cool to 110 °C over 12 h. After this heat treatment procedure, the transmission was measured in the dehydrated state immediately after the samples had been taken out of the furnace and cooled to room temperature. This heat treatment procedure allows us to maintain the samples in a dry state for the dehydrated state measurements after each heating step while avoiding cracking of the samples due to excessive heating or cooling rates. The samples were then rehydrated in deionised H₂O for 48 h

and the transmission was measured in the rehydrated state. After this, the samples were heated to the next higher temperature and the measuring protocol was repeated. This sequence was continued with 50 °C steps until 600 °C. All transmission measurements were acquired at room temperature.

Results

‘Water’ species and porosity in silcrete

The NIR spectra of silcrete show the two expected combination bands near 5200 cm^{-1} (H_2O) and 4400 cm^{-1} (SiOH) (Fig. 1). The shape and frequencies of both bands are similar in samples WK-13-11 and WK-13-13. Sample WK-13-08 has a significantly higher ‘water’ concentration, its SiOH band has a different shape and its H_2O band a different frequency (c.f. Fig. 1). It is noteworthy that, despite their different shapes, all SiOH bands can be fitted with four components, three of which lie at the same frequencies in the three samples (4535, 4450 and 4273 cm^{-1}). While the absorbance of the H_2O band in the hydrated state is significantly greater than in the dehydrated state, as can be expected, the absorbance of the SiOH band shows the opposite trend. This may be caused by band overlap with the water bands on both high- and low-frequency sides of the silanol band. Differing H-bond strength in the hydrated and dehydrated states, which would influence the SiOH absorption coefficient, can be ruled out because the components of the SiOH bands remain at the same frequencies in both states for all three samples (compare Fig. 1a, b). The concentrations of structural H_2O , SiOH and the volume of pore space in the three samples are shown in Table 1.

Thermal behaviour of the ‘water’ species and porosity

The H_2O and SiOH combination bands of WK-13-11 and WK-13-08 after heating to different temperatures are shown in Fig. 2a–d, and the complete set of spectra recorded from WK-13-08 after heating to all temperature steps are shown in the supplementary file for an overview. The intensity of the SiOH bands decreases progressively upon heating. Figure 3 shows the SiOH concentration in the three silcrete samples plotted as a function of heating temperature. Most of the silanol is lost between 300 and 450 °C. Its concentration is reduced by $\approx 80\%$ in WK-13-08, by $\approx 60\%$ in WK-13-11 and by $\approx 40\%$ in WK-13-13 indicating that the initial concentration influences the percentage that can be lost during heating. Figure 4 shows H_2O concentrations in the dehydrated state plotted as a function of the heating temperature. WK-13-08 shows the clearest thermal

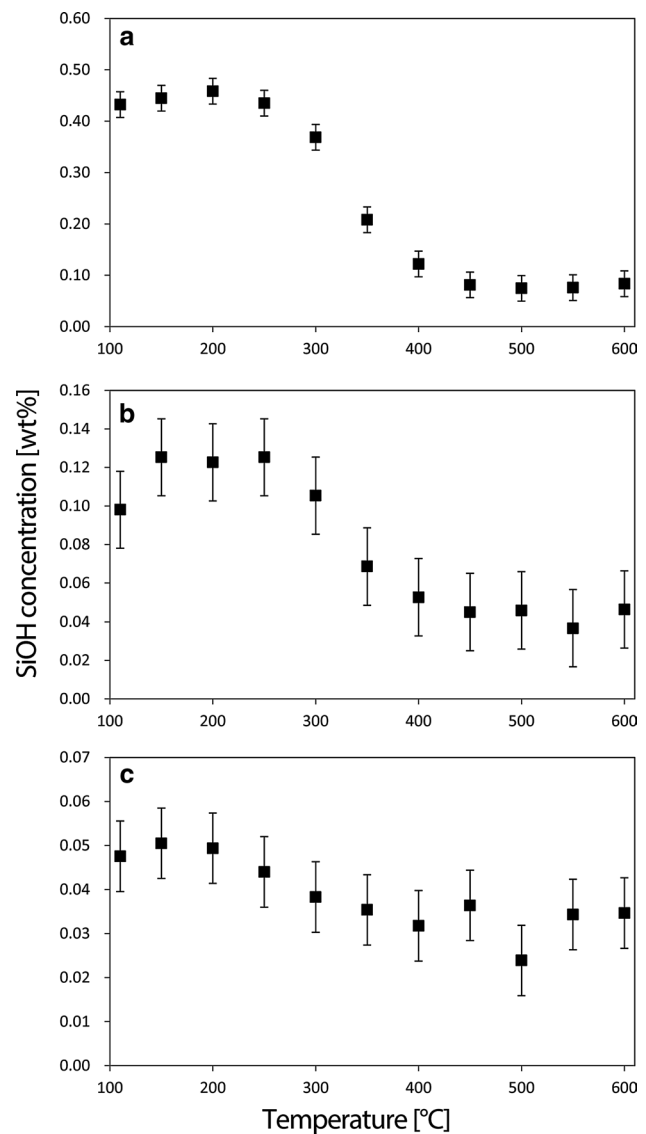


Fig. 3 Plots of the loss of SiOH in dehydrated silcrete samples. The SiOH concentration in wt%, as calculated from the integral absorbance of the SiOH combination band near 4400 cm^{-1} in dehydrated samples, is plotted against the annealing temperature. **a** WK-13-08, **b** WK-13-11, **c** WK-13-13

evolution outside of the measurement error. The concentration of H_2O tightly held in the structure increases between 300 and 400 °C and water is lost above 450 °C. The loss of H_2O can also be observed in WK-13-11 above 400 °C. Error bars of the measurements of WK-13-13 are too large to show a clear trend. When plotted one against the other, the SiOH and structural H_2O values of WK-13-08 below the onset of H_2O loss at 450 °C show a linear regression with $r^2 = 0.96$, indicating a strong correlation (inlet in Fig. 4a). The wavenumber of the dehydrated state H_2O bands does not change significantly after heating to different temperatures in WK-13-11 and in WK-13-13 and no clear change

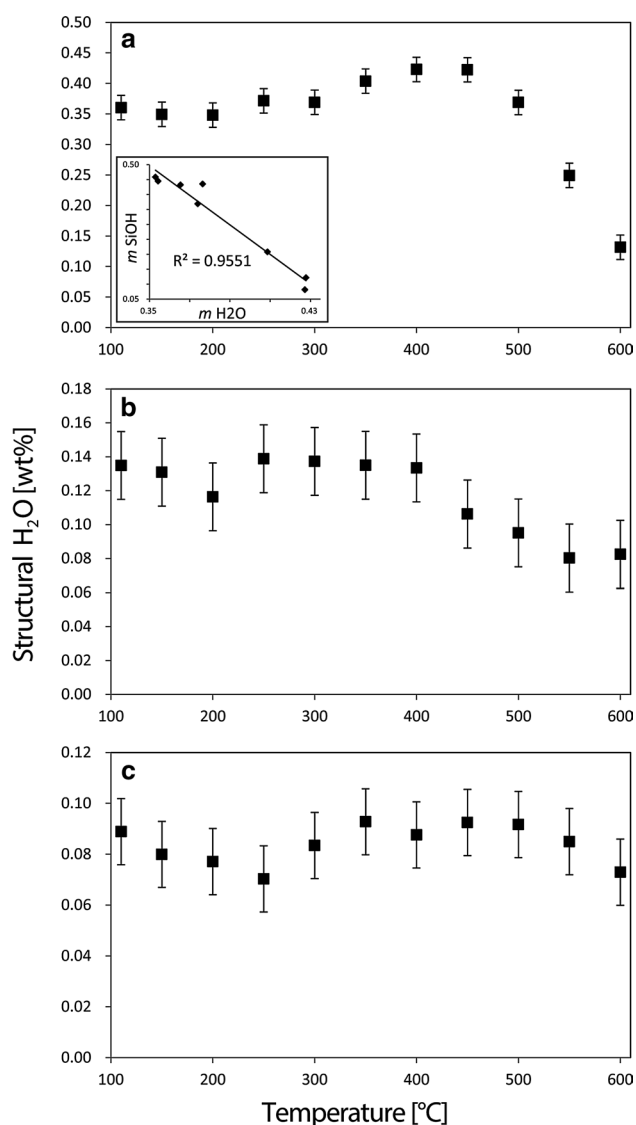


Fig. 4 Plots of the thermal evolution of H₂O tightly held in the structure of silcrete samples. The H₂O concentration in wt%, as calculated from the linear absorbance of the H₂O combination band near 5200 cm⁻¹ in dehydrated samples, is plotted against the annealing temperature. **a** WK-13-08, **b** WK-13-11, **c** WK-13-13. The *inset* in (a) shows the H₂O concentration between 110 and 450 °C plotted against SiOH of WK-13-08 to highlight the linear correlation between both values

in H₂O band shape could be observed in the spectra of these two samples. In sample WK-13-08 the H₂O band may be interpreted to slightly shift to lower wavenumbers (Fig. 2c) although this trend cannot be seen in WK-13-11 (Fig. 2a). Figure 5 shows the evolution of the samples' pore space. While WK-13-08 shows no thermal evolution, the pore space of WK-13-11 is reduced above 250 °C and increases again above 400 °C. Error bars of the measurements of WK-13-13 are too large to be affirmative, but the curve can also be interpreted to be U-shaped as for WK-13-11.

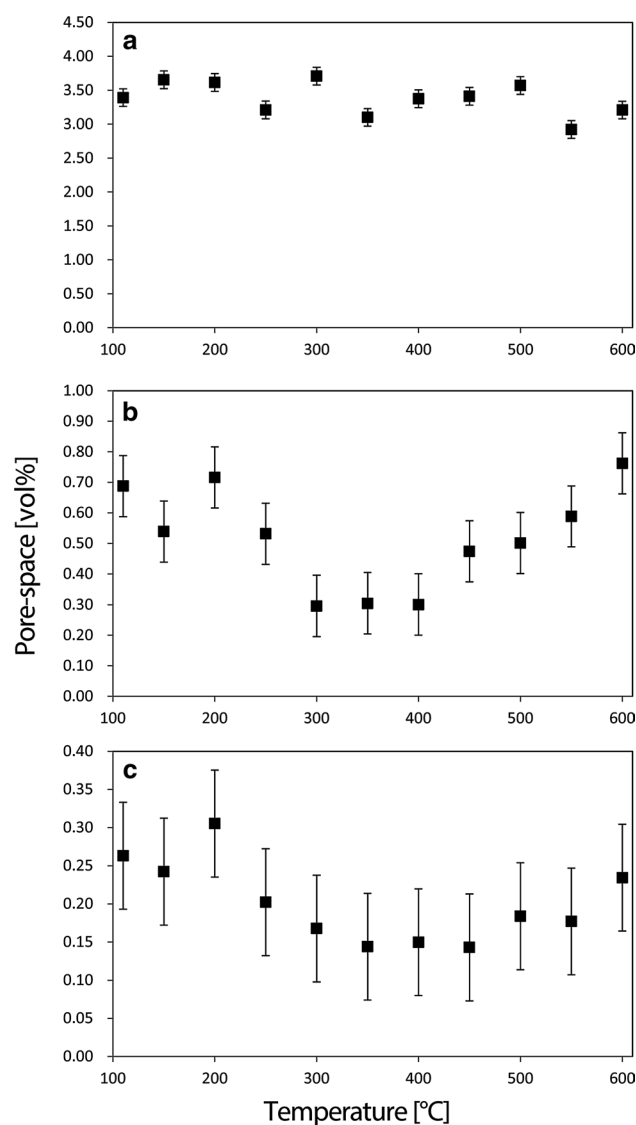


Fig. 5 Plots of the thermal evolution of intergranular pore space in silcrete samples. The pore space in vol%, as calculated from the mass of H₂O loosely held in intergranular pores, is plotted against the annealing temperature. The equation for this calculation is given in “Samples and experimental protocol” section of the text. **a** WK-13-08, **b** WK-13-11, **c** WK-13-13

Figure 6 documents the appearance of isolated SiOH in the dehydrated silcrete samples as expressed by the fundamental SiOH stretching band at 3740 cm⁻¹ (Fig. 2e). Silanol that is not or almost not involved in H-bonding begins to appear between 400 and 450 °C. For WK-13-08 and WK-13-11, these temperatures are correlated with the onset of structural water loss, suggesting that part of the SiOH is H-bound to H₂O in silcrete. No free SiOH can be seen in the spectra of rehydrated samples. Figure 7 shows the thermal evolution of the H-bonding strength of SiOH groups as expressed through the ratio between high- and low-energy components of the SiOH combination band. Figure 7a–c

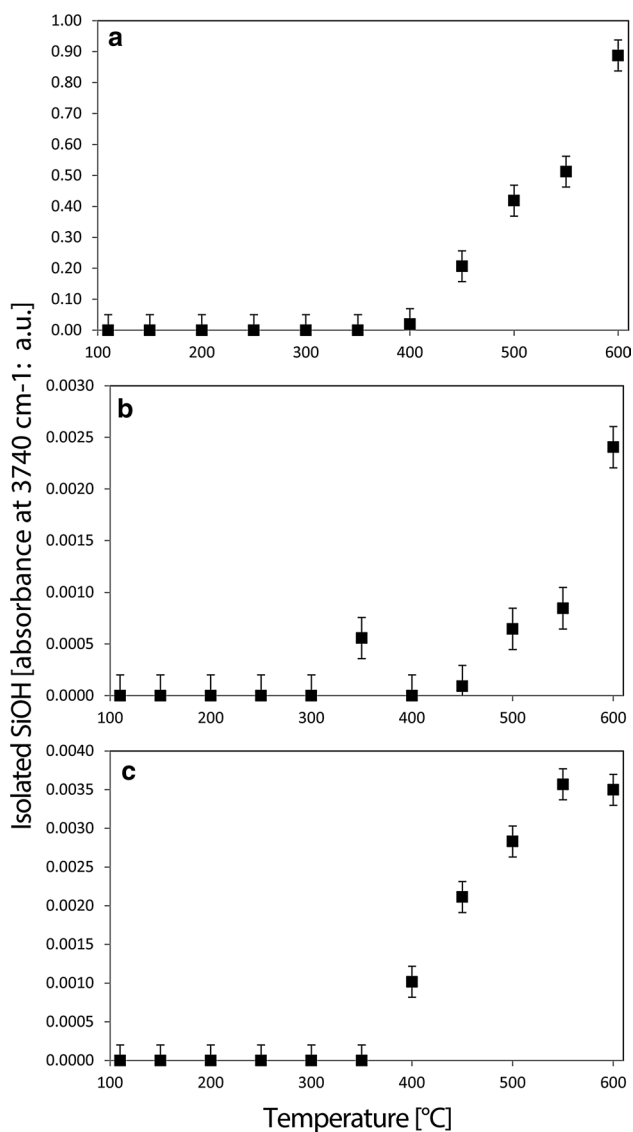


Fig. 6 Plots showing the appearance of isolated SiOH, not involved in H-bonding, at temperatures above 400 °C in silcrete samples. Isolated SiOH is not quantified and only the untransformed absorbance value is plotted to highlight its thermal formation. All absorbance values were measured on dehydrated state spectra. **a** WK-13-08, **b** WK-13-11, **c** WK-13-13

shows the ratio calculated on dehydrated state spectra, indicating that SiOH in silcrete begins to be less involved in H-bonding from 300 °C upward. The curve of WK-13-08 is almost an inversed curve of its SiOH loss (compare Figs. 4a, 7a), and for WK-13-08 and WK-13-11, the onset of the H-bond strength reduction is correlated with the beginning of SiOH loss. These correlations indicate that the shape of the absorption band is mainly influenced by H-bonding between neighbouring silanol groups and not between SiOH and H₂O. Figure 7d shows the thermal evolution of the ratio in hydrated state spectra. While for WK-13-13 no

clear evolution can be seen, the curves of WK-13-08 and WK-13-11 demonstrate the progressive isolation of SiOH from 250 °C on and the gradual increase in H-bond strength from 450 °C upward, indicating that H₂O can re-enter the structure after heating to elevated temperatures.

Discussion

Precision of the measurements and errors

The absolute ‘water’ contents we determined in our analyses should be regarded as semi-quantitative only. Errors in the concentrations of H₂O and SiOH are expected to arise from the used imprecise absorption coefficients, uncertainties of the baselines used for absorbance measurements and overlap of the combination bands with neighbouring absorptions. Although a previous study on a variety of silica polymorphs, using infrared spectroscopy and thermogravimetry, indicates that the NIR protocol we applied in this work is not too far from the samples’ real water contents (Schmidt et al. 2013b), a reliable absolute H quantification must await further studies using neutron scattering. However, the relative evolution of the signal, after heating to different temperatures, is expected to be reliable because all factors that potentially cause errors are the same for the measurements of the different temperature steps. Another factor that may be expected to influence the quantification of OH in silcrete is hydroxyl in clay. Clay is, however, unlikely to influence the relative measurement of OH in silcrete at successive temperatures because OH in most clay minerals is stably held up to temperatures above 550 °C or even higher (Grim 1962). It also appears highly unlikely that OH in clay influences the measurement of OH in our silcrete samples at all: The powder diffraction data obtained during the preparation of this study (Lauer 2014) did not show any clay minerals and, although oriented samples are needed to quantify clay using XRD, the overall concentration of clay minerals can be expected to be very low in the three studied samples. Hydroxylated TiO₂ may potentially also be misidentified as hydroxyl in quartz by our protocol. However, the overall low anatase concentrations in the three samples (XRD patterns revealed <0.5 wt% in all three samples, Lauer 2014) cannot be expected to contribute significantly to the SiOH combination band measured in silcrete. Even if the entire surface of the anatase grains is hydroxylated, the overall addition to the silcrete’s total content in OH remains low. Although only detailed future studies can shed light on the role of hydroxyl in TiO₂, we expect it to contribute only very marginally, if at all, to the measured percentage of OH in bulk silcrete samples. A third factor of uncertainty is that

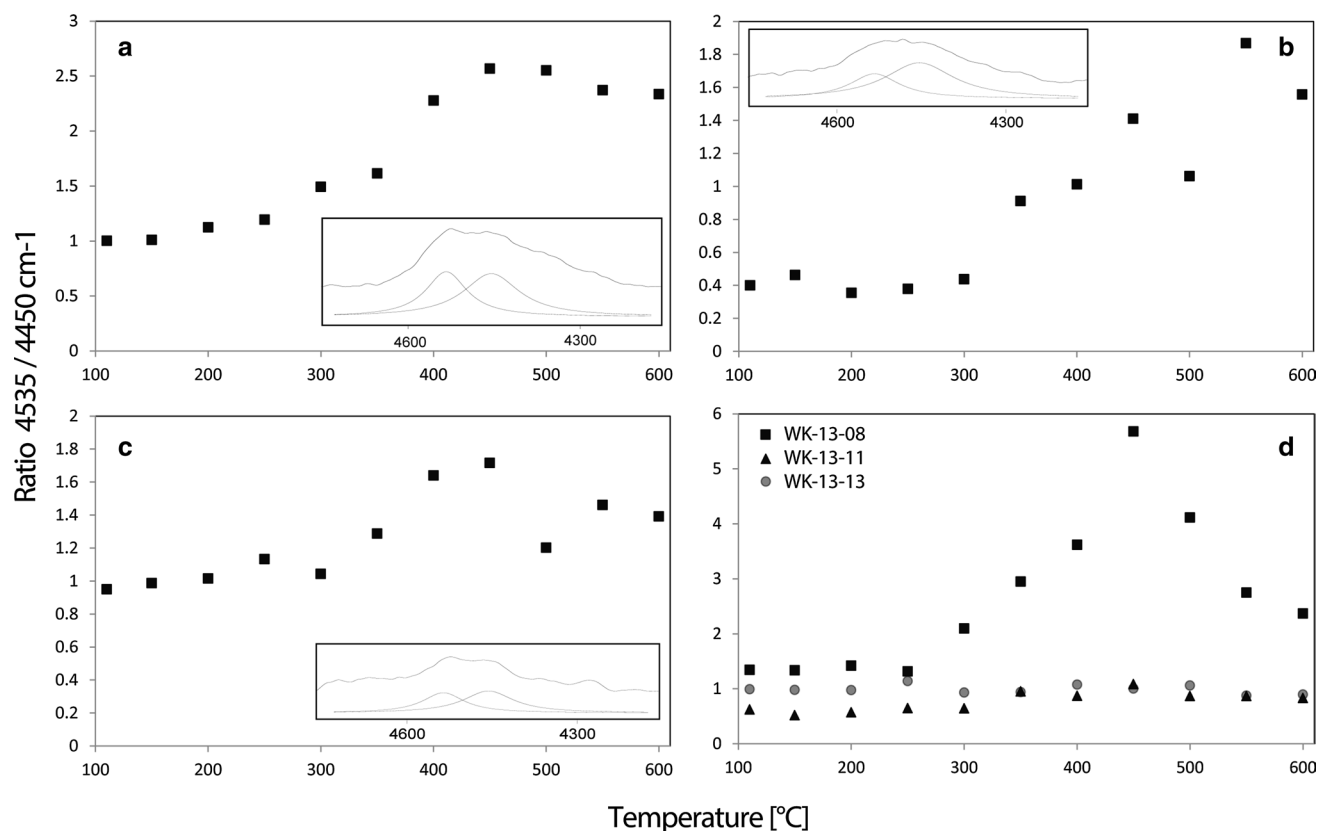


Fig. 7 Plots showing the reduction in H-bond strength of silanol. The implication of silanol in H-bonding is expressed by the ratio between two components of the SiOH combination band at 4535 and 4450 cm⁻¹. The other two components used to fit the whole SiOH absorption envelope (see text) were not interpreted in this study and

are not shown in the *insets* of (a–c). Measurements in the dehydrated state: **a** WK-13-08, **b** WK-13-11, **c** WK-13-13. The *inlets* show these two components obtained by best fit models of the absorption envelope. Measurements of the ratio in the hydrated state are shown in (**d**)

the measured silanol NIR signal can be expected to be of hybrid origin (clasts + cement). As quantitatively summarised in Table 1, all three samples consist of two generations of quartz, older quartz clasts derived from the regolith and younger microquartz cement. Frondel (1982) identified two types of OH inclusion in quartz, depending among other factors on the formation temperature of the quartz crystals (Types A and B). High-temperature quartz (Frondel's Type A quartz) was reported to show a somewhat more complex absorption spectrum in the range of the mid-infrared fundamental H₂O absorption band than low-temperature crystals (Frondel's Type B). Although silcrete's cement can be expected to be of low-temperature origin, the quartz clasts may be of Type A quartz, potentially disturbing the signature of OH measured by our analyses. However, the NIR signature of OH in Type A quartz remains unknown and only future studies will allow to shed light on the role of structural OH in quartz clasts in silcrete. As it stands, the silanol loss we measured must be regarded as overall average of the whole rocks.

Thermal evolution of porosity

Our data contradict the thermal behaviour of open pores in silcrete proposed by Schmidt et al. (2013a). They showed a reduction in open pores at temperatures above 400 °C, which led them to affirm that higher temperatures were more favourable for silcrete heat treatment. Based on our more precise results, this cannot be maintained. We noted either no evolution of the pore space at all or an increase in pores above 400 °C. On the other hand, our data fully support Schmidt et al.'s results concerning the maximum tolerated heating rate. Even though pores were lost during the first stages of heating of the two samples with lower initial pore volume, they never disappeared completely. Water evaporation remains therefore possible even after heat treatment, preventing the build-up of excessive vapour pressure that may cause overheating of silica rocks when they are heated with fast ramp rates (Schmidt 2014). These temperatures and the tolerance for fast ramps appear to be independent of the type of silcrete. Samples with more clasts than matrix contain less pore space but also less water to be

evaporated; inversely, samples with more matrix and therefore more water that must be evaporated also have a significantly larger pore space.

Heat-induced fracturing

When hydroxyl in SiOH reacts with H₂O, part of it is trapped in the structure of the rocks. This H₂O is only released above 400 °C or even 450 °C, most likely by internal fracturing that creates a secondary open pore space. The growth of pore volume above 400 °C in WK-13-11 and WK-13-13 supports this (Fig. 5b, c). No thermal evolution of pore space can be noted in sample WK-13-08 (Fig. 5a). This might be due to the high initial value of ≈3.5 vol%, masking a possible weak evolution. However, the silanol–H-bond strength in this sample does suggest the appearance of internal fractures above 450 °C: the high-temperature augmentation of hydrogen-bond strength in the hydrated sample (Fig. 7d, above 450 °C in d) suggests that water entering the rock can access new, previously shielded, silanol groups with which it can now bond. Hence, new open pores are created. The appearance of isolated silanol in the dehydrated state (Fig. 6) also supports the internal fracturing model by indicating that, in dehydrated samples, SiOH on newly created internal surfaces are not in contact with H₂O or SiOH anymore. Free silanol disappears when the samples are rehydrated, indicating hydroxylation of the new surfaces (accounting for new Si–OH···OH–Si bonds) and the contact of water with these surfaces (forming Si–OH···OH₂ bonds).

New Si–O–Si bonds

It has been shown that SiOH loss results in the formation of new Si–O–Si bonds in chalcedony and quartz single crystals (Graetsch et al. 1985; McLaren et al. 1983; Schmidt et al. 2011). Whether this is also the case in silcrete cannot be answered unambiguously by our study. No explicit spectroscopic data that could prove bond formation are available for silcrete because the mid-infrared vibration of non-bridging Si–O (Schmidt and Fröhlich 2011) was not analysed in our experimental set-up. However, from a theoretical point of view it appears clearly that the loss of SiOH causes free charges that must be satisfied by either rehydroxylation or the formation of siloxane. Our data on the SiOH loss show that, like in chalcedony (Graetsch et al. 1985; Schmidt et al. 2011), the reduction in silanol in silcrete is at least partly irreversible, strongly suggesting the formation of Si–O–Si. Further studies about the crystallinity of quartz in silcrete after heat treatment or ²⁹Si NMR studies of the silicon bonding behaviour should shed further light on this matter.

Hence, the ‘water’-related thermal transformations of silcrete are the same as in chalcedony bearing silica rocks (chert). However, heating parameters such as the activation energy, the maximum temperature, the ramp rate and maybe even the reaction kinetics are different in silcrete. Ideal temperatures for the heat treatment of silcrete are expected to lie somewhere above the minimal activation temperature for SiOH loss and below the internal fracture threshold. Ramp rates can be significantly faster than in finer-grained chalcedony.

Conclusion

The water-related thermal transformations in silcrete, as investigated by our NIR spectroscopic study of different ‘water’ species, and their parameters are as follows:

Ideal heating temperatures the first transformation to take place in silcrete is the loss of silanol from 250 to 300 °C on. This silanol reacts with molecular water, part of which is trapped in the structure of the rocks, but another larger part of which can be freely evaporated through the large network of intergranular open pores. This reaction goes on for approximately 200 °C. Thus, concerning the ‘water’-related thermal transformations, temperatures between 250 and 450 °C appear to be ideal for silcrete heat treatment.

Heating rates regardless of the maximum temperatures, silcrete can be heat-treated with relatively fast ramp rates. The reason for this is that water evaporation is made easy by the relatively large network of open pores leading to the surface. This network of pores is not totally closed during heat treatment. It prevents critical vapour pressure, which otherwise would lead to heat-induced fracturing, up to at least 450 °C.

Excessive temperatures the SiOH loss is essentially terminated at 450 °C making it useless to heat-treat silcrete with temperature above this threshold. Temperatures much higher than this may even be disadvantageous for heat treatment. This is because water is progressively liberated from closed pores above 450 °C. This water evaporation is associated with internal fracturing, opening up new pores, which can be expected to create heterogeneities in the silcrete and degrade its knapping quality. However, it can be expected that this degradation of knapping quality remains minimal at heating temperatures that are only slightly above the fracturing threshold (450–500 °C) because the onset of internal fractures is progressive.

Whether there are other processes, not related to water, that play a role during silcrete heat treatment needs to be investigated in future studies. Also, a thorough study of the temperature dependent evolution of the mechanical properties of silcrete should shed light on the correlation between ‘water’ and some of the key values such as elasticity and fracture toughness that play an important role during stone knapping.

Acknowledgments We thank the Deutsche Forschungsgemeinschaft (DFG) for funding of the research project *Heat Treatment in the South African MSA* that made the present study possible (Grant No: CO 226/25-1, MI 1748/2-1, NI 299/25-1) and for funding the Agilent Cary 660 spectrometer used for parts of this study (MI 1748/1-1). We also thank Junichi Fukuda and an anonymous reviewer for their corrections and suggestions during the review process for this publication.

References

- Aines RD, Rossman GR (1984) Water in minerals? A peak in the infrared. *J Geophys Res* 89:4059–4071. doi:[10.1029/JB089iB06p04059](https://doi.org/10.1029/JB089iB06p04059)
- Anderson jr JH (1965) Calorimetric vs. infrared measures of adsorption bond strengths on silica. *Surf Sci* 3:290–291
- Anderson jr JH, Wickersheim KA (1964) Near infrared characterization of water and hydroxyl groups on silica surfaces. *Surf Sci* 2:252–260
- Benesi HA, Jones AC (1959) An infrared study of the water–silica gel system. *J Phys Chem* 63:179–182. doi:[10.1021/j150572a012](https://doi.org/10.1021/j150572a012)
- Binder D (1984) Systèmes de débitage laminaire par pression: exemples chasséens provençaux. In: Tixier J, Inizan ML, Roche H (eds) *Préhistoire de la pierre taillée, 2: économie du débitage laminaire: technologie et expérimentation: IIIe table ronde de technologie lithique*. Meudin-Bellevue, october 1982. Cercle de Recherches et d’Etudes Préhistoriques, Paris, pp 71–84
- Bordes F (1969) Traitement thermique du silex au Solutréen. *Bull Soc Préhist Fr* 66:197
- Brown KS et al (2009) Fire as an engineering tool of early modern humans. *Science* 325:859–862
- Cochrane GWG, Habgood PJ, Doelman T, Herries AIR, Webb JA (2012) A progress report on research into stone artefacts of the southern Arcadia Valley, central Queensland. *Aust Archaeol* 75:104–109
- Corkill T (1997) Red, yellow and black: colour and heat in archaeological stone. *Aust Archaeology* 45:54–55
- Crabtree DE, Butler BR (1964) Notes on experiment in flint knapping: I heat treatment of silica materials. *Tebawa* 7:1–6
- Eriksen BV (2006) Colourful lithics—the “Chaîne Opératoire” of Heat Treated Chert Artefacts in the Early Mesolithic of Southwest Germany. In: Kind CJ (ed) *After the ice age. Settlements, subsistence and social development in the Mesolithic of Central Europe, Materialhefte zur Archäologie in Baden-Württemberg*. Stuttgart: Konrad Theiss Verlag, pp 147–153
- Flörke OW, Köhler-Herbertz B, Langer K, Tönges I (1982) Water in microcrystalline quartz of volcanic origin: agates. *Contrib Miner Petrol* 80:324–333
- Flörke OW, Graetsch H, Martin B, Roller K, Wirth R (1991) Nomenclature of micro- and non-crystalline silica minerals, based on structure and microstructure. *Neues Jahrb Miner Abh* 163:19–42
- Frondel C (1982) Structural hydroxyl in chalcedony (type B quartz). *Am Mineral* 67:1248–1257
- Fukuda J, Peach CJ, Spiers CJ, Nakashima S (2009) Electrical impedance measurement of hydrous microcrystalline quartz. *J Mineral Petrol Sci* 104:176–181. doi:[10.2465/jmps.081022f](https://doi.org/10.2465/jmps.081022f)
- Graetsch H, Flörke OW, Miede G (1985) The nature of water in chalcedony and opal-C from brazilian agate geodes. *Phys Chem Miner* 12:300–306
- Grim R (1962) *Applied clay mineralogy*. International series in the earth sciences. McGraw-Hill, New York
- Hanckel M (1985) Hot rocks: heat treatment at Burrill Lake and Currarong, New South Wales. *Archaeol Ocean* 20:98–103
- Hiscock P (1993) Bondian technology in the Hunter Valley, New South Wales. *Archaeol Ocean* 28:65–76
- Kronenberg AK (1994) Hydrogen speciation and chemical weakening of quartz. In: Heaney PJ, Prewitt CT, Gibbs GV (eds) *Silica: physical behaviour, geochemistry and materials applications*. Reviews in Mineralogy 29. Mineralogical Society of America, Washington, pp 123–176
- Langer K, Flörke OW (1974) Near infrared absorption spectra (4000–9000 cm⁻¹) of opals and the role of “water” in these SiO₂·nH₂O minerals. *Fortschr Mineral* 53:17–51
- Lauer C (2014) *Tempern von Silcrete—Liegt der Verbesserung der Zuschlagbarkeit derselbe Mechanismus zugrunde wie bei Flint?* Unpublished Bachelor thesis, Eberhard Karls University of Tübingen
- Léa V (2005) Raw, pre-heated or ready to use: discovering specialist supply systems for flint industries in mid-Neolithic (Chassey culture) communities in southern France. *Antiquity* 79:1–15
- McDonald RS (1958) Surface functionality of amorphous silica by infrared spectroscopy. *J Phys Chem* 62:1168–1178. doi:[10.1021/j150568a004](https://doi.org/10.1021/j150568a004)
- McLaren AC, Cook RF, Hyde ST, Tobin RC (1983) The mechanisms of the formation and growth of water bubbles and associated dislocation loops in synthetic quartz. *Phys Chem Miner* 9:79–94. doi:[10.1007/bf00308151](https://doi.org/10.1007/bf00308151)
- Merciecia A, Hiscock P (2008) Experimental insights into alternative strategies of lithic heat treatment. *J Archaeol Sci* 35:2634–2639
- Micheelsen H (1966) The structure of dark flint from Stevns, Denmark. *Medd Dansk Geol Foren* 16:285–368
- Mourre V, Villa P, Henshilwood CS (2010) Early use of pressure flaking on lithic artifacts at Blombos Cave, South Africa. *Science* 330:659–662
- Porraz G, Texier P-J, Archer W, Piboule M, Rigaud J-P, Tribolo C (2013) Technological successions in the Middle Stone Age sequence of Diepkloof Rock Shelter, Western Cape, South Africa. *J Archaeol Sci* 40:3376–3400. doi:[10.1016/j.jas.2013.02.012](https://doi.org/10.1016/j.jas.2013.02.012)
- Roberts DL (2003) Age, genesis and significance of south african coastal belt silcretes, Memoir 95. Council for Geoscience, Pretoria
- Roqué-Rosell J et al. (2010) Influence of heat treatment on the physical transformations of flint used by neolithic societies in the Western Mediterranean. In: International conference, materials research society, Boston, 2010. pp mrsf10-1319-ww1309-1302
- Rowney MAASC (1994) Palaeomagnetic tests of heat treated silcrete artefacts. *Aust Aborig Stud* 1:39–43
- Schmidt P (2011) *Traitement thermique des silicifications sédimentaires, un nouveau modèle des transformations cristallographiques et structurales de la calcédoine induites par la chauffe*. Unpublished doctoral thesis, Muséum national d’histoire naturelle
- Schmidt P (2014) What causes failure (overheating) during lithic heat treatment? *Archaeol Anthropol Sci* 6:107–112. doi:[10.1007/s12520-013-0162-3](https://doi.org/10.1007/s12520-013-0162-3)
- Schmidt P, Fröhlich F (2011) Temperature dependent crystallographic transformations in chalcedony, SiO₂, assessed in mid infrared spectroscopy. *Spectrochim Acta Part A Mol Biomol Spectrosc* 78:1476–1481

- Schmidt P, Mackay A (2016) Why was silcrete heat-treated in the middle stone age? An early transformative technology in the context of raw material use at Mertenhof Rock Shelter, South Africa. *PLoS ONE* 11:e0149243. doi:[10.1371/journal.pone.0149243](https://doi.org/10.1371/journal.pone.0149243)
- Schmidt P, Badou A, Fröhlich F (2011) Detailed FT near-infrared study of the behaviour of water and hydroxyl in sedimentary length-fast chalcedony, SiO₂, upon heat treatment. *Spectrochim Acta Part A Mol Biomol Spectrosc* 81:552–559
- Schmidt P et al (2012) Crystallographic and structural transformations of sedimentary chalcedony in flint upon heat treatment. *J Archaeol Sci* 39:135–144
- Schmidt P, Porraz G, Slodczyk A, Bellot-gurlet L, Archer W, Miller CE (2013a) Heat treatment in the South African Middle Stone Age: temperature induced transformations of silcrete and their technological implications. *J Archaeol Sci*. doi:[10.1016/j.jas.2012.10.016](https://doi.org/10.1016/j.jas.2012.10.016)
- Schmidt P, Slodczyk A, Léa V, Davidson A, Puaud S, Sciau P (2013b) A comparative study of the thermal behaviour of length-fast chalcedony, length-slow chalcedony (quartzine) and moganite. *Phys Chem Miner* 40:331–340. doi:[10.1007/s00269-013-0574-8](https://doi.org/10.1007/s00269-013-0574-8)
- Schmidt P et al (2015) A previously undescribed organic residue sheds light on heat treatment in the Middle Stone Age. *J Hum Evol* 85:22–34
- Scholze H (1960) Über die quantitative UR-spektroskopische Wasserbestimmung in Silikaten. *Fortschr Mineral* 38:122–123
- Summerfield MA (1983) Petrography and diagenesis of silcrete from the Kalahari Basin and Cape coastal zone, Southern Africa. *J Sediment Res* 53:895–909
- Tiffagom M (1998) Témoignages d'un traitement thermique des feuilles de laurier dans le Solutrén supérieur de la grotte du Parpalló (Gandia, Espagne) *Paléo* 10:147–161
- Wilke PJ, Flenniken J, Ozbun TL (1991) Clovis Technology at the Anzick Site, Montana. *J Calif Great Basin Anthropol* 13:242–272